Available online at www.sciencedirect.com
ScienceDirect
Journal of Power Sources 161 (2006) 1412–1419
JOURNAL OF POWER SOURCES
www.elsevier.com/locate/jpowsour

Secondary current density distribution analysis of an aluminum–air cell

Shaohua Yang [a,b,*], Weiqian Yang [a], Gongquan Sun [a], Harold Knickle [b]

[a] *Direct Alcohol Fuel Cell Laboratory, Dalian Institute of Chemical Physics, Chinese Academy of Science, Dalian 116023, China*
[b] *Department of Chemical Engineering, University of Rhode Island, Kingston, RI 02881, USA*

Received 10 March 2006; received in revised form 28 April 2006; accepted 28 April 2006
Available online 12 June 2006

Abstract

Secondary current density distributions in a parallel two-plane Al/air cell and a wedge shaped Al/air cell were analyzed. The parameters studied include the entrance effect, the activity of the cathode, the cell gap and the extension of the cathode. The entrance effect disappears at about a one to two cell gap from the entrance. The activity of the cathode has a large effect on the local current density. With increases in the cell gap, the average current density decreases, but the peak current density over the average current density increases. By extending the cathode below the anode, the high local current density can be reduced. In a wedge shaped Al/air cell, the planar portion of the anode enters the cell. As the anode is consumed, the top portion of the anode is consumed faster because of the decreased cell gap and increased reaction rate. The anode adapts to be parallel to the cathode in the cell. A FEMLAB (finite element method) package was used for all the calculations.

Keywords: Aluminum/air cell; Secondary current distribution; FEMLAB

1. Introduction

An aluminum/air battery system has the potential to be used to produce power to operate vehicles [1,2]. In our previous paper, cell performance model equations were provided [3–5]. Of particular interest in the design of the cell is the edge effect where a high local current density ("hot spot") exists and can damage the cathode [6].

The current density and potential distribution depend on the geometry (the field equation), the conductivity of the solution, the activation overpotential, the concentration overpotential and special effects in and near the electrodes [7]. In many applications, not all of these factors are taken into account. This results in a classification of current distributions: primary, secondary and tertiary distributions. When all kinds of overpotentials can be neglected, we say that the current distribution is a primary distribution. When only the activation overpotentials are important, the obtained current distribution is called the secondary distribution. When concentration effects become important, the concentration is taken into account together with the activation overpotential, and the current distribution is said to be a tertiary distribution. Table 1 summarizes the classification of these current distributions. Table 2 shows the relative values of different overpotential losses for four cell gaps. Table 2 shows calculations at a cell voltage of 0.8 V and an electrolyte velocity of 8 cm s^{-1} [5].

From the analysis results in our previous paper, it can be concluded that, for an aluminum/air cell in a typical operating range of current density, the concentration polarization effect can be overlooked. Thus a study of the secondary current distributions along the electrodes is important. In this paper, the secondary current distributions in a parallel two plane and a wedge shaped aluminum/air cell were calculated using a FEMLAB (finite element method) package [8]. The parameters studied included the entrance effect, the activity of the cathode, the cell gap and the cathode extension.

2. Model

2.1. Model equations

The potential field in the electrolyte can be expressed by the following equation (without concentration polarization):

$$\nabla(\kappa\nabla\Phi) = 0, \tag{1}$$

* Corresponding author. Tel.: +86 411 84379063; fax: +86 411 84379063.
E-mail address: yangsh@dicp.ac.cn (S. Yang).

0378-7753/$ – see front matter © 2006 Elsevier B.V. All rights reserved.
doi:10.1016/j.jpowsour.2006.04.143

Nomenclature

a	empirical cathode kinetic constants in Eq. (15) ($A\,m^{-2}\,V^{-1}$)
b	empirical cathode kinetic constants in Eq. (15) ($A\,m^{-2}$)
a'	empirical cathode kinetic constants in Eq. (12) ($m^2\,V\,A^{-1}$)
b'	empirical cathode kinetic constants in Eq. (12) (V)
E_{eq}	cell equilibrium voltage (V)
F	Faraday's constant (96,500 C equiv.$^{-1}$)
i_a	anode current density ($A\,m^{-2}$)
i_c	cathode current density ($A\,m^{-2}$)
i_{a0}	exchange current density of the anode reaction ($A\,m^{-2}$)
R	ideal gas constant ($J\,mol^{-1}\,K^{-1}$)
S	cell gap (m)
T	temperature (K)
V_{cell}	cell voltage (V)
x	cathode extension below the anode (m)
X	cathode extension in dimensionless form, $X = x/S$

Greek symbols

α_m	empirical anode kinetic constants
η_a	activation overpotential of anode (V)
η_c	activation overpotential of cathode (V)
η_1, η_2	overpotenial of electrodes 1 (anode) and 2 (cathode) (V)
κ	conductivity of electrolyte at certain gas fraction in the electrolyte ($S\,m^{-1}$)
κ^0	conductivity of electrolyte at gas fraction = 0 ($S\,m^{-1}$)
Φ	solution potential (V)
Φ_a	solution potential just outside the anode (V)
Φ_c	solution potential just outside the cathode (V)

where κ is the conductivity of the electrolyte ($\kappa = \kappa_0$); Φ is the electrolyte potential.

The boundary conditions for Eq. (1) are:

$$(-\nabla(\kappa\nabla\Phi)n) = i_a \quad \text{at the anode} \tag{2}$$

and

$$(-\nabla(\kappa\nabla\Phi)n) = -i_c \quad \text{at the cathode,} \tag{3}$$

$$(-\nabla(\kappa\nabla\Phi)n) = 0$$

$$\text{at other boundaries } (i = 0 \text{ is an insulating condition}) \tag{4}$$

where i_a and i_c are the current density into the bulk electrolyte, and can be expressed in terms of the potential relationships at both electrodes.

The current density distributions were obtained by solving Eq. (1) with the boundary conditions using the finite element package FEMLAB.

2.2. Development of the current density boundary conditions

From our previous work [4,5], we know that at the anode:

$$\Phi_a = E_{eq} - V_{cell} - \eta_1 \tag{5}$$

or

$$\eta_1 = E_{eq} - V_{cell} - \Phi_a \tag{6}$$

If there is no concentration polarization:

$$\eta_1 = \eta_A. \tag{7}$$

And the anode kinetics can be written as:

$$i_a = i_{a0} \exp\left[\left(\frac{\alpha_m F}{RT}\right)\eta_a\right] \tag{8}$$

Combining Eqs. (6)–(8), we get

$$i_a = i_{a0} \exp\left[\left(\frac{\alpha_m F}{RT}\right)(V_{eq} - V_{cell} - \Phi_a)\right] \quad \text{at the anode.} \tag{9}$$

Similarly, at the cathode

$$\Phi_c = -\eta_2. \tag{10}$$

If there is no concentration polarization at the cathode:

$$\eta_2 = \eta_c; \tag{11}$$

Table 1
Current distribution classification

Current distribution	Activation overpotential	Concentration overpotential
Primary	No	No
Secondary	Yes	No
Tertiary	Yes	Yes

Table 2
Cell overpotential and ohmic losses at 0.8 V and 8 cm s^{-1} velocity [5]

Cell gap (cm)	Current density ($A\,m^{-2}$)	Activation loss anode (V)	Activation loss cathode (V)	Ohmic loss (V)	Total loss (V)
0.2	5280	1.32 (68.4%)	0.47 (24.4%)	0.14 (7.2%)	1.93 (100%)
0.4	4370	1.25 (64.7%)	0.45 (23.7%)	0.23 (11.6%)	1.93 (100%)
0.6	3810	1.20 (62.2%)	0.43 (22.2%)	0.30 (15.6%)	1.93 (100%)
0.8	3380	1.16 (60.1%)	0.42 (21.8%)	0.35 (18.1%)	1.93 (100%)

Table 3
Constants used for FEMLAB modeling [5,9]

Anode kinetic parameters	Cathode kinetic parameters	Operating conditions	Other constants
$\alpha_m = 0.07956$	$a = 3.898 \times 10^4\ A\ m^{-2}\ V^{-1}$	$T = 333\ K$	$R = 8.314\ J\ mol^{-1}\ K^{-1}$)
$i_{a0} = 137.1\ A\ m^{-2}$	$b = -1.3094 \times 10^4\ A\ m^{-2}$	$V_{cell} = 0.9–1.3\ V$	$F = 96{,}500\ C\ equiv.^{-1}$, $\kappa_0 = 80\ S\ m^{-1}$, $E_{eq} = 2.726\ V$

and assume linear profile, the cathode kinetics can be written as:

$$\eta_c = a' i_c + b', \tag{12}$$

where a' and b' can be obtained by fitting experimental data.

Alternatively, the experimental data can be fitted to determine these coefficients by:

$$i_c = \left(\frac{1}{a'}\right)\eta_c - \frac{b'}{a'}. \tag{13}$$

Combining Eqs. (10), (11) and (13), gets

$$i_c = \left(\frac{-1}{a'}\right)\Phi_c - \frac{b'}{a'} \tag{14}$$

or

$$i_c = a\Phi_c + b \quad \text{(linear profile)} \quad \text{at the cathode,} \tag{15}$$

where $a = -1/a'$ and $b = -b'/a'$.

2.3. Modeling calculation procedures

The modeling calculation procedures for secondary current distributions using FEMLAB are:

(1) Choose the "PDE" (Eq. (1)) in Model Navigator, select "2D", and select "Conductive media DC" from the Multiphysics menu;
(2) Draw the geometry;
(3) Set the boundary conditions (Eqs. (2) and (3));
(4) Add constants (see Tables 3 and 4) and expressions (Eqs. (9) and (15));
(5) Initialize the mesh;
(6) Solve the problem;
(7) If necessary, resize the mesh and solve again.

The parameters used in these modeling calculations are given in Tables 3 and 4.

Table 4
Cathode kinetic parameters for Eq. (6) [5,9,10]

Cathode	Kinetic parameters	
	$a/104\ A\ m^{-2}\ V^{-1}$	$b/104\ A\ m^{-2}$
AC65 Yardney (Ag)	1.3106	−0.4409
AC75 Yardney (CoTMPP)	1.1806	−0.2832
AC78 Yardney (Pt)	1.3210	−0.3342
Chan and Savinell	3.898	−1.3094

3. Secondary current distribution in a parallel two-plane cell

In this section, the potential distribution in a parallel two-plane cell for three different voltages is calculated. The current density distribution was also calculated for three cathode extensions, three cell voltages, five cathode activities and four cell gaps. The cathode extensions were chosen to minimize the entrance effects due to high current density. The cell voltages were chosen in the normal operating range of interest. The activities of the cathode cover the ranges available in industrial cathodes. Cell gaps were chosen to cover the possible range of interest in a practical Al–air cell.

3.1. Potential distribution

In the entrance region, there is a sharp current density change in the 1–2 times cell gap range below and above the entrance. The mesh size used in FEMLAB is refined to make the current distribution curve smoother.

The potential distribution for a parallel two-plane cell design is shown in Figs. 1–3 at cell voltages of 0.9, 1.1 and 1.3 V, respectively. The maximum value of the potential at the anode decreases with increasing cell voltage. The ohmic loss decreases with increasing cell voltage from 0.114 to 0.053 V. The figures clearly show the existence of a potential variation below the cell entrance. These figures also show that the potential becomes linear at about 0.0015–0.002 m above the entrance.

The potential contour at each cell voltage is shown in Figs. 4–6, respectively. Figs. 4–6 visualize the cell potential dependence on position. From Fig. 4, it can be seen that at about a 1 cell gap, the potential lines (example: at $\Phi = 0.5378$ V) become vertical. They no longer depend on the horizontal position. Curvature of the equal potential lines disappears at about

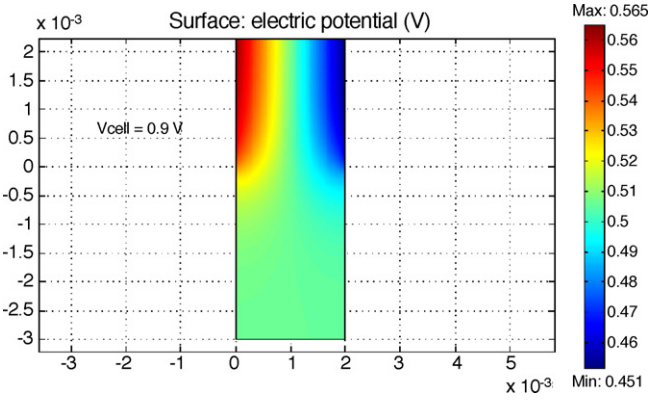

Fig. 1. The potential distribution in the electrolyte of a parallel two-plane Al/air cell with anode and cathode equal size at a cell voltage of 0.9 V.

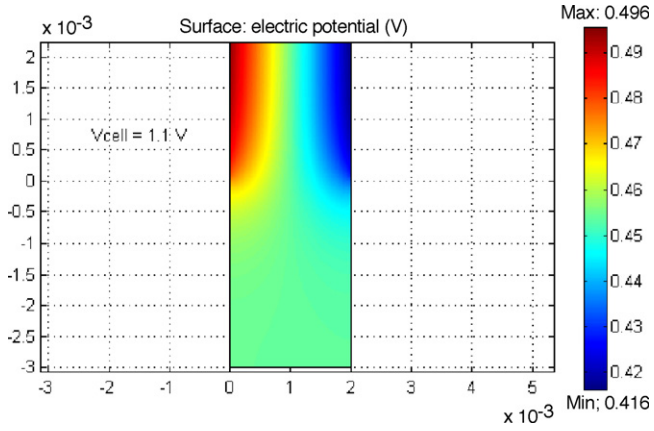

Fig. 2. The potential distribution in the electrolyte of a parallel two-plane Al/air cell with anode and cathode equal size at a cell voltage of 1.1 V.

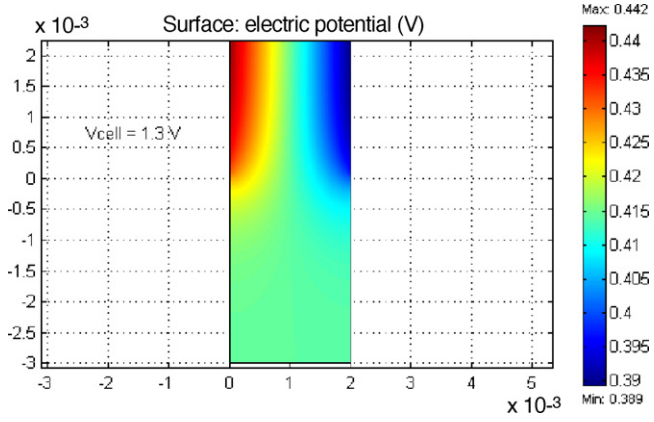

Fig. 3. The potential distribution in the electrolyte of a parallel two-plane Al/air cell with anode and cathode equal size at a cell voltage of 1.3 V.

0.002 m from the entrance. The constant potential lines below the entrance clearly show curvature and the current density below the entrance is not zero. From Figs. 5 and 6, similar results can be obtained.

Potential distributions at cell heights of 0.002, 0.003, 0.004 m in Figs. 7–9 were obtained by analysis of the potential contour at a cell voltage of 0.9 V (see Fig. 4). From Figs. 7–9, it can be seen that the potential distributions at cell heights of 0.003–0.004 m

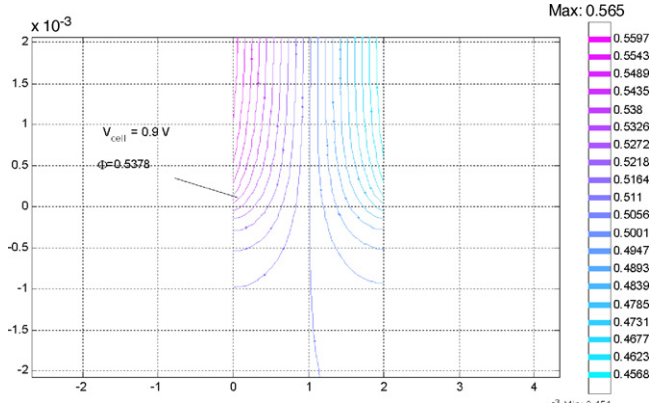

Fig. 4. The potential contour in the electrolyte of a parallel two-plane Al/air cell with anode and cathode equal size at a cell voltage of 0.9 V.

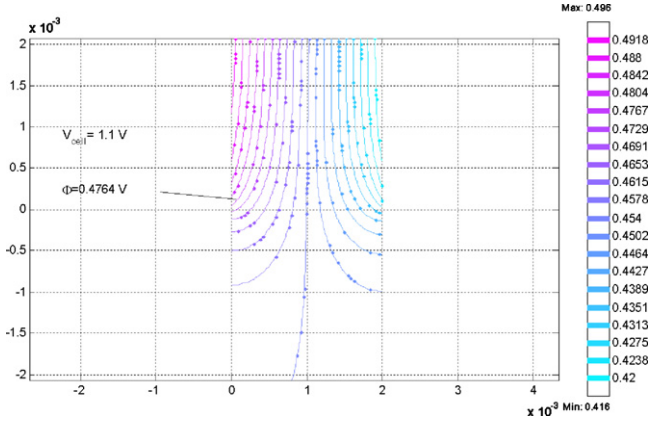

Fig. 5. The potential contour in the electrolyte of a parallel two-plane Al/air cell with anode and cathode equal size at a cell voltage of 1.1 V.

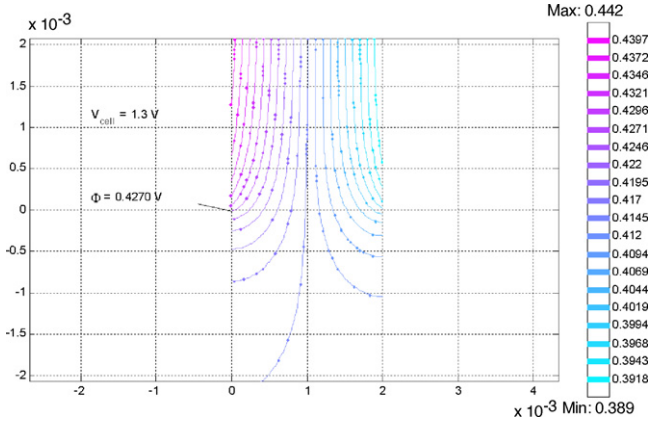

Fig. 6. The potential contour in the electrolyte of a parallel two-plane Al/air cell with anode and cathode equal size at a cell voltage of 1.3 V.

(1.5–2 cell gap) are linearly dependent on the distance from the anode, i.e. as the entrance effect disappears, the problem becomes one-dimensional.

3.2. *Effect of the cathode extension on current distribution*

At the entrance, the local current density is much higher than the average current density. The high local current density ("hot

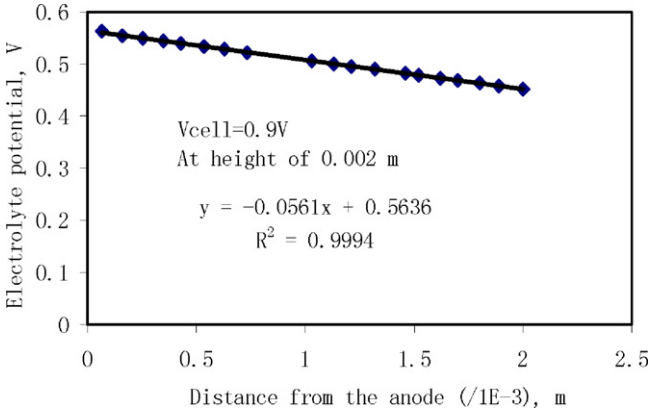

Fig. 7. Electrolyte potential distribution with anode and cathode equal size at a cell voltage of 0.9 V and a cell height of 0.002 m.

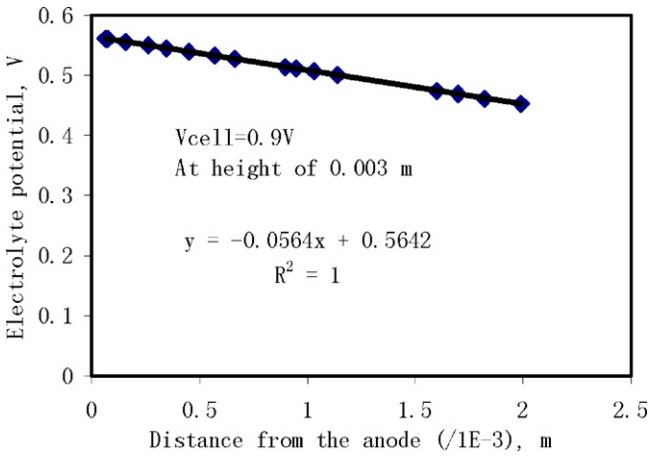

Fig. 8. Electrolyte potential distribution with anode and cathode equal size at a cell voltage of 0.9 V and a cell height of 0.003 m.

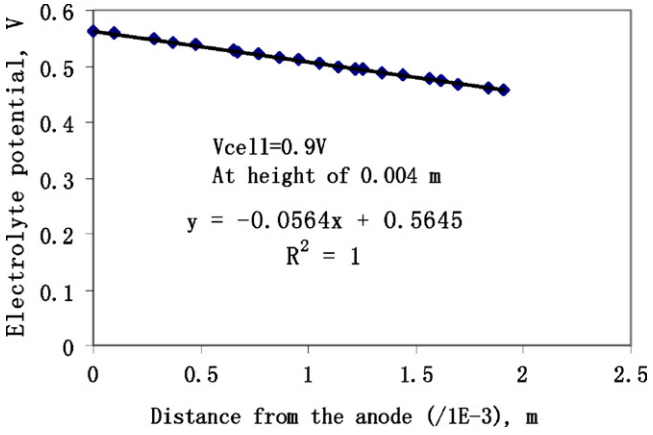

Fig. 9. Electrolyte potential distribution with anode and cathode equal size at a cell voltage of 0.9 V and a cell height of 0.004 m.

spot") is harmful and might damage the cathode. To avoid the high local current density, geometrical factors were studied. The cathode extension was defined in dimensionless form as: $X = x/S$; x is the extension of the cathode below the anode and S is the cell gap. From Fig. 10, it can be seen that, when the anode and cathode are of equal size, there is very high local current density

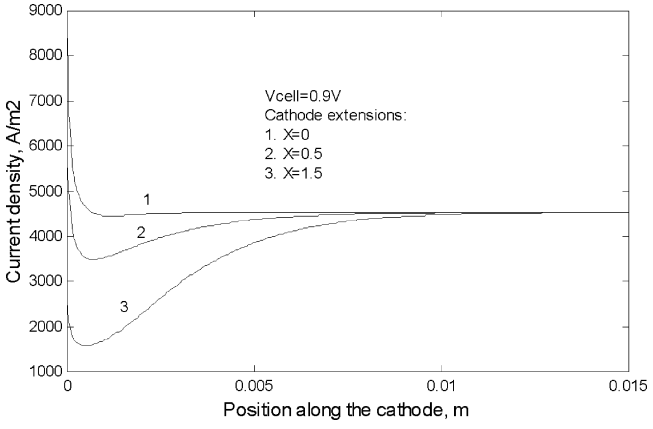

Fig. 10. Effect of cathode extension on the current distribution.

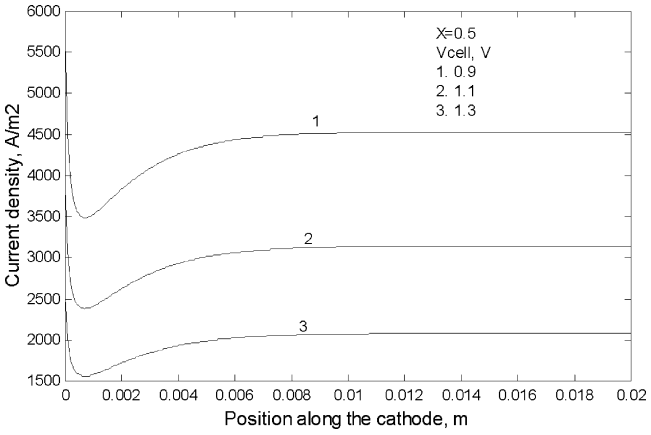

Fig. 11. Current density distribution at different cell voltages. $X = 0.5$.

at the entrance (peak current density/average current density is about 1.8); At $X = 0.5$ and 1.5, the high local current density is reduced, and at $X = 1.5$, the local current density is smaller than the current density away from the entrance.

3.3. Current density distribution at different cell voltages

Fig. 11 shows the current density distribution at different cell voltages at $X = 0.5$. At higher cell voltages (1.1–1.3 V), the high local current density is reduced at $X = 0.5$, but at lower cell voltage (0.9 V), the local current density is reduced but still higher than the current density away from the entrance. So at a lower cell voltage (0.9 V) a further extension is needed to reduce the high local current density.

3.4. Effect of the cathode activity on the current distribution

From Eq. (4), $i = a\Phi + b$, one can see that "a" is related to the activity (reaction rate) of the cathode, i.e., at a given Φ, when "a" is bigger, the current density is higher. In other words, when "a" is bigger, the overpotential of the cathode is smaller at a fixed current density. The results shown in Fig. 12 are obtained when the value of "a" was changed from $1/5a$ to $5a$ while keeping the "b" value unchanged. It can be seen that, with increases in

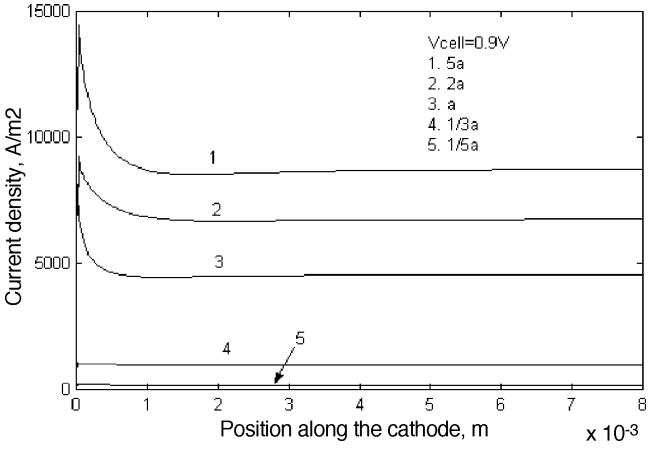

Fig. 12. Effect of cathode activity on current density distribution at $X = 0$.

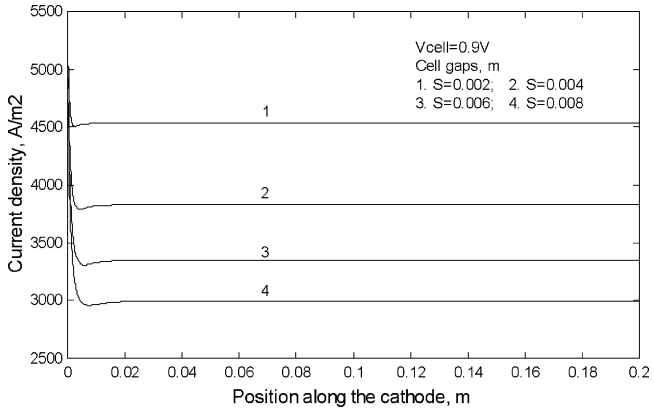

Fig. 13. Effect of cell gap on current density distribution at $X = 0$.

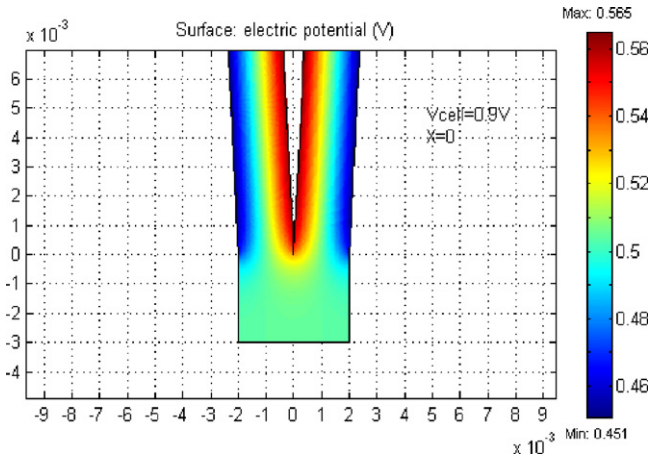

Fig. 14. The electrolyte potential distribution in a wedge-type Al/air cell with no cathode extension ($X = 0$).

cathode activity (increasing "*a*"), the local current density and also the current density away from the entrance, will increase and the local current density is very high. The peak current density/average current density is as high as 1.8.

3.5. Effect of the cell gap on the current density distribution

Fig. 13 shows that with increases in the cell gap, the average current density decreases but the peak current density over the average current density increases. The peak current density over the average current density for cases 1 to 4 is: 1.21, 1.37, 1.53, and 1.69, respectively. Thus, reducing the cell gap will increase the cell performance, i.e. increase the average current density and decrease the peak current density over the average current density value at a fixed cell voltage.

3.6. Summary

In Section 3.1, the potential distributions in the electrolyte were analyzed. We found that the potential distributions at cell heights of about 1–2 cell gaps are linearly dependent on the distance from the anode, i.e. the entrance effect disappears, and the problem becomes one-dimensional.

In Sections 3.2–3.5, the secondary current density distribution in a parallel two-plane Al/air cell was analyzed. The activity of the cathode has a large effect on the local current density. With increases in the cell gap, the local current density increases, but the increase is not as significant as the increase in the current density away from the entrance. By extending the cathode (0.5–1.5 cell gap), the local high current density can be reduced. With a lower cell voltage (high current density), a greater extension is needed to reduce the local current density to below the current density above the entrance.

4. Secondary current distribution in a wedge shape cell

An aluminum/air battery system can provide cars with range and acceleration characteristics similar to those of internal combustion engines [1,11]. One important requirement of this system for electric vehicle applications is rapid refueling of the Al anode fuel. A wedge shaped cell configuration has been designed. The aluminum anode is fed into the battery and adapts a wedge shape and is completely consumed [12]. We calculated the secondary current distribution along the anode and the cathode in a wedge-type design at different cell gaps, cathode extension and cathode activity.

4.1. Potential distribution

For a wedge-type cell design, there is a sharp current density change near the entrance, at about 1–2 cell gap range below and above the entrance. The geometry mesh size used in FEMLAB was refined to make the current distribution curve smoother. The angle in the apex of the anode was kept at 5°.

The potential distribution for the wedge-type cell design is shown in Fig. 14 from which we can see that at a distance along the height of the electrodes of 1–2 cell gaps above the entrance, the potential distribution becomes more uniform. Thus the entrance effect is only important in that range.

4.2. Effect of the cell gap on cell performance

If we ignore the entrance effect, a wedge shaped cell is essentially the same as a parallel two plane, aluminum/air cell. Table 5 shows the effect of the cell gap on the cell current density at cell voltages of 0.9, 1.1 and 1.3 V. These values of cell voltages were chosen as representative of the operating conditions of the cell. For a fixed cell voltage, the current density decreases when the cell gap increases. At a fixed cell gap, when the cell voltage

Table 5
Average current density in the electrolyte at different cell gap at various operating cell voltages

Cell gap ($\times 10^{-3}$ m)	Current density (A m^{-2})		
	0.9 V	1.1 V	1.3 V
2	4550	3150	2120
4	3750	2750	1890
6	3300	2470	1740
8	2980	2250	1610

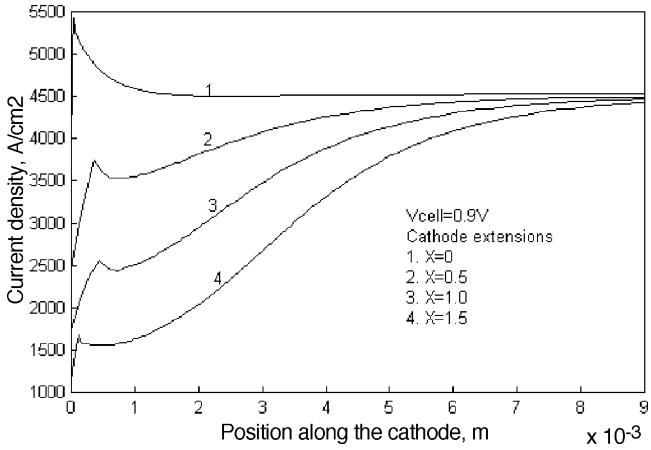

Fig. 15. Current density distribution along the cathode at different cathode extensions.

increases, the current density decreases as expected. For example, at a cell voltage of 0.9 V, when the cell gap increases from 0.002 to 0.008 m, about 33.3% of the current density is lost. Reducing the cell gap increases the cell performance. A minimum cell gap is required for laminar flow of the electrolyte. The results in Table 3 are consistent with our previous results [5].

4.3. Effect of the cathode extension on the current density distribution

Fig. 15 shows the entrance effects on the current distribution along the cathode when the cathode is extended below the anode. At $X=0$ (equal size of anode and cathode), high local current density occurs in the range of about 1 cell gap (0.002 m) from the entrance (peak current density/average current density is about 1.20). At $X>0.5$ (an extension of half a cell gap), the locally high current density is reduced and is lower than the current density away from the entrance.

4.4. Effect of the cathode activity on the current distribution

It can be seen from Fig. 16 that with increases in cathode activity, the local current density and also the current density away from the entrance will increase and the local current density is very high. The peak current density/average current density is about 1.44, 1.21, 1.17, 1.1, and 1.0, respectively for cases 1–5 (see Table 6). The results are similar to that of a two plane, parallel Al/cell, but the peak local current density is lower than that of a parallel two-plane Al/cell (see Fig. 5).

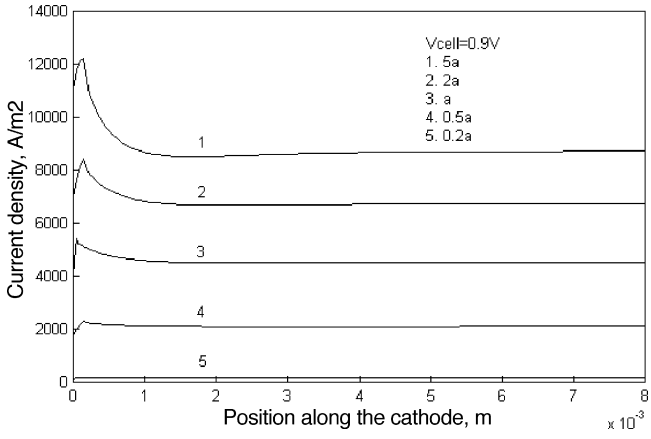

Fig. 16. Effect of cathode activity on current density distribution. *a* changes from 0.2*a* to 5*a*.

Table 6
Effect of cathode activity on peak current density over average current density

a values	Peak current density/average current density
0.2*a*	1.0
0.5*a*	1.1
a	1.17
2*a*	1.21
5*a*	1.44

a changes from 0.2*a* to 5*a*.

4.5. Current distribution along the anode with varying cell gaps

Fig. 17 shows the current density distribution along the anode with the cell gap decreasing with the cell height (see Fig. 18 for a schematic of a wedge-type aluminum/air cell). In this case, the entrance effect is not taken into account. If the anode becomes thicker, the cell gap becomes smaller and the current density increases. Thus, the anode is consumed faster when the anode is thicker (i.e. at smaller cell gaps). With time the anode will adapt to the wedge-type shape.

4.6. Summary

In this section, the secondary current density distribution in a wedge shape cell was analyzed. The effects of cell gap, activity and cathode extensions on the current density distribution along the cathode are similar to those of the parallel two-plane design, with the peak local current density lower. It was also shown that the anode is consumed faster when the anode is thicker (i.e. at a smaller cell gap) causing the anode to adapt to the wedge shape.

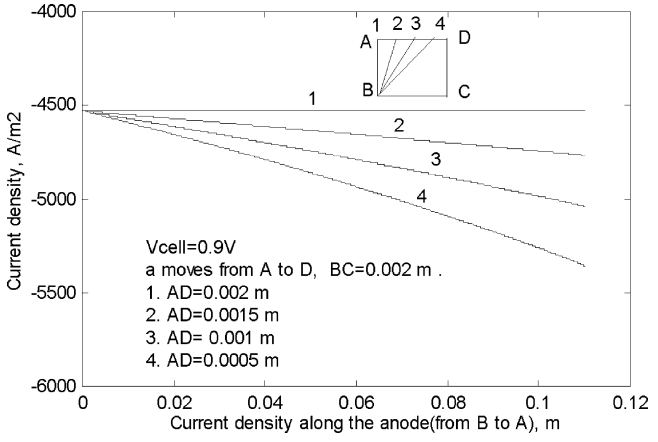

Fig. 17. Current density distribution along the anode (from B to A) with varying cell gaps. BA is the anode height and CD is the cathode height.

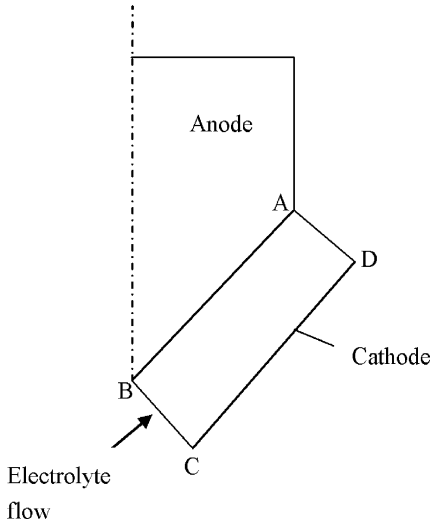

Fig. 18. Schematic of a wedge-type aluminum/air cell.

5. Conclusions

Potential distributions in the electrolyte of a parallel two-plane Al/air cell were calculated. It was found that the potential distributions at cell heights above 0.003–0.004 m (1.5–2 cell gap height range) are linearly dependent on the distance from the anode. At those heights, the entrance effect disappears and the problem becomes one-dimensional.

Current density distributions in a parallel two-plane Al/air cell were also analyzed. The activity of the cathode was found to have a large effect on the local current density near the cathode. This activity depends upon the reaction rate and the overpotential. With increases in the cell gap, the average current density decreases, but the peak current density over the average current density increases. By extending the cathode below the anode by 0.5–1.5 cell gaps, the local high current density can be reduced.

The current density distribution in a wedge shape cell was also analyzed. The results showed that the effects of the cell gap, the activity and cathode extension on the current density distribution along the cathode are similar to those of the parallel two-plane design. The peak local current density is lower than that in the parallel two-plane case. The anode is consumed faster where the anode is thicker (at a smaller cell gap) because of the higher reaction rate at fixed cell voltages. The reaction rate difference causes the anode to adapt to the wedge shape.

High local current at the cathode edge which is detrimental to cathode life is affected both by geometric and kinetic factors. To protect the cathode and ensure a long lifetime, the cathode should be slightly oversized compared to the anode by 1.5–2 cell gaps height range in a practical design for an Al/air cell and battery. Modeling equations and a FEMLAB package using the finite element method were presented here and are useful tools for analysis of the secondary current distribution and a prediction of the cell performance of the Al/air cell and battery.

References

[1] S. Yang, H. Knickle, Design and analysis of aluminum/air battery system for electric vehicles, J. Power Sources 112 (2002) 162–173.
[2] S. Yang, H. Knickle, Aluminum/air electric vehicle life cycle analysis, in: Proceedings of the 202nd Meeting of the Electrochemical Society, Salt Lake City, UT, USA, October 20–24, 2002.
[3] S. Yang, H. Knickle, Effect of cell gap on current density distribution in an aluminum/air cell, in: Proceedings of the 204th Meeting of the Electrochemical Society, Orlando, FL, USA, October 12–16, 2003.
[4] S. Yang, H. Knickle, Two dimensional transport modeling of an aluminum/air cell, in: Proceedings of the 203rd Meeting of the Electrochemical Society, Paris, France, April 27–May 2, 2003.
[5] S. Yang, H. Knickle, Modeling analysis of the performance of an aluminium–air cell, J. Power Sources 124 (2003) 572–585.
[6] R.F. Savinell, G.G. Chase, Analysis of primary and secondary current distributions in a wedge-type aluminum cell, J. Appl. Electrochem. 18 (1988) 499–503.
[7] J. Deconinck, Current distributions and electrode shape changes in electrochemical systems, in: C.A. Brebbia, S.A. Orszag (Eds.), Lecture Notes in Engineering, Springer-Verlag, 1992.
[8] Comsol Company, FEMLAB, Multiphysics in MATLAB, September 2003, http://www.comsol.com.
[9] K.Y. Chan, R.F. Savinell, Modeling calculations of an aluminium–air cell, J. Electrochem. Soc. 138 (1991) 1976–1984.
[10] Alupower, AC78 Technical Data Sheet, September 2002, http://www.yardney.com.
[11] H. Knickle, X. Zhang, Analysis and design of a novel control method for aluminum/air battery system, in: Proceeding of the 204th Meeting of the Electrochemical Society, Orlando, FL, USA, October 12–16, 2003.
[12] D.A.J. Rand, Batteries for Electric Vehicles, Research Studied Press Ltd., 1998.